NJC

Accepted Manuscript

This is an *Accepted Manuscript*, which has been through the Royal Society of Chemistry peer review process and has been accepted for publication.

Accepted Manuscripts are published online shortly after acceptance, before technical editing, formatting and proof reading. Using this free service, authors can make their results available to the community, in citable form, before we publish the edited article. We will replace this *Accepted Manuscript* with the edited and formatted *Advance Article* as soon as it is available.

You can find more information about *Accepted Manuscripts* in the Information for Authors.

Please note that technical editing may introduce minor changes to the text and/or graphics, which may alter content. The journal's standard Terms & Conditions and the Ethical guidelines still apply. In no event shall the Royal Society of Chemistry be held responsible for any errors or omissions in this *Accepted Manuscript* or any consequences arising from the use of any information it contains.

ROYAL SOCIETY OF CHEMISTRY

www.rsc.org/njc

Journal Name

RSCPublishing

ARTICLE

SnO_2 nanotube arrays embedded in a carbon layer for high-performance lithium-ion battery applications

Cite this: DOI: 10.1039/x0xx00000x

Ji Hyun Um,[ab] Seung-Ho Yu,[ab] Yong-Hun Cho*[c] and Yung-Eun Sung*[ab]

Received 00th January 2012,
Accepted 00th January 2012

DOI: 10.1039/x0xx00000x

www.rsc.org/

A facile strategy for preparing one-dimensional (1D) SnO_2 nanotube arrays embedded in a carbon layer (C-SnO_2 NTs) has been developed via a sol-gel method using polycarbonate (PC) as a template. The introduction of a carbon layer carbonized from a PC membrane at the top of a SnO_2 nanotube arrays results in the SnO_2 nanotubes standing on the current collector and preserving their 1D structure without an aggregation between each other, which enables their direct application to the anode of lithium-ion batteries. The binder- and carbon-free C-SnO_2 NTs as a self-supporting anode exhibits a stable and high reversible capacity of 500 mAh g^{-1} at 0.1 A g^{-1} after 40 cycles. The improved Li ion storage and stable capability are attributed to the 1D hollow structure, alleviating the large volume changes of SnO_2 and enhancing electron and Li ion diffusion transport in the nanotube.

Introduction

By growing demand in various applications of lithium-ion batteries (LIBs), development of high-performance materials with higher energy and power density and better cycling stability has been stimulated, leading to the significant progress in high capacity anode materials such as Sn and Si compared to commercially used graphite limited by a theoretical capacity of 372 mAh g^{-1}.[1,2]

Recently, SnO_2 materials have attract great attention as anode materials due to their high theoretical capacity (~781 mAh/g), natural abundance, and low cost. However, the practical application of SnO_2 materials is impeded by poor capacity retention resulting from inherently large volume changes (~300%) during Li ion insertion and extraction.[2,3] Substantial efforts are devoted to relieve the large volume changes causing pulverization of active material and electrical contact loss with the current collector. Therefore, quite good cyclability was obtained for SnO_2-based electrode materials at present,[3,4,5] which enables the expansion to flexible[6,7] and thin film battery[8] application. Moreover, carbon coating has proven to be effective to improve the capacity retention and rate capability of electrode materials for LIBs. It is well-known that carbonaceous materials maintain the electrical conductivity as a conductive agent, and at the same time, the volume changes of active materials during cycling are absorbed, which results in obvious improvement of cycle performance. There are various researches on the carbon coating such as core-shell,[9-11] embedded,[5] and scaffold[12] structure.

One-dimensional (1D) nanostructures have fascinating advantages compared to their bulk counterparts, and demonstrate their improved performance such as Si,[13] SnO_2,[14] Co_3O_4,[15] Fe_2O_3,[16] and TiO_2[17] anodes. In particular, nanotubes grown directly on current collector substrate are expected to having the following advantages.[18-20] First, since each nanotube is connected to the current collector, every nanotube contributes to the capacity, and also binder or conductive additives are not required. Second, the tubular structure has a large interior void space to accommodate the volume change stresses. Third, the open end and thin wall structures allow for more efficient Li ion diffusion at exterior and interior surfaces, which enables more symmetric volume changes and larger charge storage. Furthermore, direct channels for efficient electron pathways enhance charge transport. Among the various synthetic strategies to prepare the nanotubes, template-assisted approach is widely explored and demonstrated to be an excellent method including nanofibers,[21] CNTs,[22] composite nanowires,[23,24] anodic aluminum oxide (AAO),[25] and polycarbonate (PC) membrane[26,27] template.

Herein, SnO_2 nanotube arrays embedded in carbon layer (C-SnO_2 NTs) were prepared by using PC membrane as a template combined with sol-gel coating method. By introducing a carbon layer carbonized from PC membrane at the top of SnO_2 nanotube

arrays, we obtained the SnO_2 nanotubes standing directly on the current collector substrate, and preserving their 1D structure without an aggregation between each other. The as-fabricated C-SnO_2 NTs, integrated with current collector and free of binder and conducting agent, was applied as a self-supporting anode for LIBs. Furthermore, the higher capacity and better cycling stability were displayed at a current density of 0.1 A g^{-1} compared to conventional powder electrode. This good performance is attributed to their 1D hollow structure, accommodating the large volume changes of SnO_2, and shortening the diffusion path of the electron and Li ion transport.

Experimental

Material synthesis

A commercially available polycarbonate (PC) membrane (with pore diameter of 200 nm, purchased from Whatman) was prepared as a template to synthesize SnO_2 nanotubes. A stainless steel (SS) foil (AISI Type 304, with thickness of 0.02 mm) was prepared from Goodfellow, and used as the current collector. The PC membrane and SS foil were punched to a size of 11 mm in diameter to fit the electrode size. The overall synthetic procedure of the C-SnO_2 NTs is schematically illustrated in Scheme 1. For a Sn-based sol of 3 M Sn(II), 0.338 g of $SnCl_2$•$2H_2O$ was dissolved in a mixture solvent consisting of 0.03 mL 37% hydrochloric acid and 0.47 mL ethanol.[26] The 3 M Sn(II) solution was subsequently aged at room temperature for 24 h. And then, triple deionized water (DI-H_2O, 0.03 mL) was added to the solution, which was aged for another 24 h. The PC with diameter of 11 mm was immersed in the prepared gel for 24 h, and put on a piece of the punched SS foil. Solvent evaporation was then conducted at 80 ℃ in vacuum. A heat treatment was carried out at 600 ℃ in an Ar atmosphere for 2 h to convert the Sn-based gel into crystalline SnO_2 and to carbonize the PC. As a final product for anode, C-SnO_2 NTs were obtained and electrochemically tested as an anode.

Characterization

X-ray diffraction (XRD) patterns were obtained with a Bruker D-5005 using Cu-Kα radiation (λ = 1.5406 Å), operating at 40 kV and 200 mA with a scan range of 10–70°. The specimen morphology was characterized using field emission scanning electron microscopy (FE-SEM), (Carl Zeiss, SUPRA 55VP). Transmission electron microscope (TEM) analysis was carried out using JEOL JEM-2100F to confirm the hollow structure. A Mettler Toledo TGA/SDTA 851 equipment was used for thermal analysis of the synthesized C-SnO_2 NTs. Sample was heated to 700 ℃ at a heating rate of 10 ℃ min^{-1} in 100 ml min^{-1} air flow. The mass of active material in each C-SnO_2 NTs electrode was obtained to five decimal places using an electronic scale by measuring the weight difference between the C-SnO_2 NTs and the SS foil. Electrochemical impedance spectroscopy (EIS) was conducted in 10 mV amplitude with the frequency range from 100 kHz to 10 mHz (Zahner, Germany).

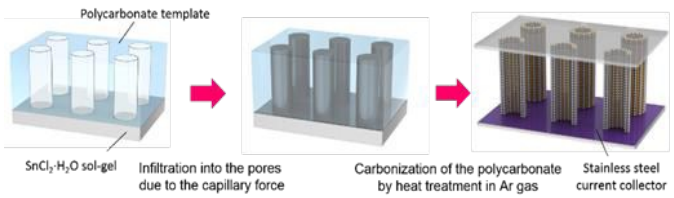

Scheme 1 Fabrication process of C-SnO_2 NTs via sol-gel method using a PC template.

Electrochemical measurement

The C-SnO_2 NTs were directly used as a working electrode and assembled into a coin cell without the addition of any binder or conductive materials, and was compared with a SnO_2 powder electrode (referred to as SnO_2 NPs) as a control group. The SnO_2 NPs were fabricated by mixing commercial SnO_2 powder (<100 nm diameter, purchased from Aldrich), polyvinylidene (PVDF) as a binder, and Ketchen Black as a conductive agent at a weight ratio of 80:10:10 in N-methyl-2-pyrrolidone (NMP) solvent. The mixed slurry was uniformly plastered onto Cu foil as a current collector via doctor blade method. The electrodes were dried under vacuum at 120 ℃ overnight and then pressed. A 2016-type coin cell consisting of the C-SnO_2 NTs (or SnO_2 NPs) as the working electrode and lithium metal as a counter and reference electrode was assembled in a glove box under a dry Ar atmosphere. The organic electrolyte used was 1.0 M $LiPF_6$ dissolved in a mixture of ethylene carbonate (EC) and diethyl carbonate (DEC) with a volume ratio of 1:1. A galvanostatic test (WBCS3000 cycler, WonA Tech, Korea) was carried out on the coin cell. All the specific capacities and current density were calculated based on the C-SnO_2 NTs mass loading.

Results and discussion

Characterization of C-SnO_2 nanotube arrays

C-SnO_2 NTs were fabricated by a simple sol-gel method using PC membrane as a template in our work. Their structural and physicochemical properties were investigated through a series of measurements. The FE-SEM image of Fig. 1a shows the synthesized SnO_2 nanotube arrays standing freely on the SS sub-

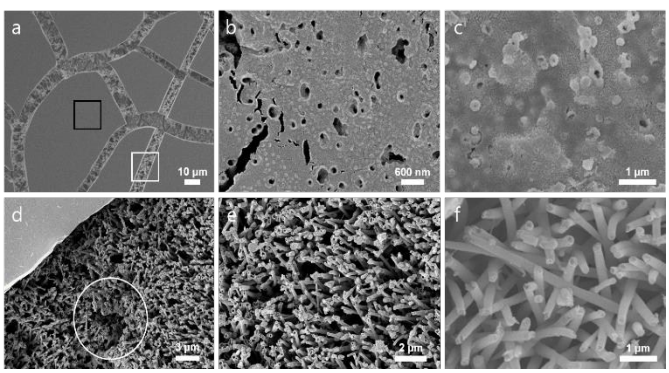

Fig. 1 FE-SEM images of (a) as-prepared C-SnO_2 NTs, (b) and (c) magnified surface morphology from a black square region in Fig. 1a, and (d)-(f) magnified surface morphology from a white square region in Fig. 1a.

strate and covered with a layer corresponding to the upper side of PC membrane. There are exposed SnO_2 nanotubes without the layer indicated by the white square region in Fig. 1a, but most SnO_2 nanotubes are under the layer. A gap between each layers is an inevitable consequence of the heat-treatment in an Ar atmosphere. As shown in Fig. 1b and c, the magnified surface morphology on the layer, enlarged from the black square region in Fig. 1a, presents a top view of the SnO_2 nanotubes embedded under the layer, and confirms *ca.* 200 nm in diameter of the SnO_2 nanotube. Fig. 1d, enlarged from a white square region in Fig. 1a, indicates again vertically grown SnO_2 nanotube arrays under the layer by observing the layer edge. Although the SnO_2 nanotubes almost grow vertically from the SS substrate and are separated apart from each other, several SnO_2 nanotubes lean and join together as indicated by a white circle region in Fig. 1d, negating the benefits of their 1D construction. In other words, the layer carbonized from the PC membrane can support the vertical growth of SnO_2 nanotubes without an aggregation between each other. Moreover, from a comparison between Fig. 1b and c and Fig. 1e and f, the layer clearly plays a role in preventing the inclined growth of SnO_2 nanotubes and assisting the development of their 1D structure. The surface composition of the C-SnO_2 NTs is identified by energy-dispersive x-ray spectroscopy (EDX). The distribution of Sn and O in Fig. S1a (ESI†) is correspond with that of C, revealing the existence of SnO_2 nanotube arrays standing under the carbonized carbon layer. EDX result of Fig. S1b (ESI†) demonstrates that the peaks of Sn, O, and C are seen in the survey spectrum, which is consistent well with the above mapping result. Meanwhile, the other elements such as Fe and Cr are as the components of SS substrate and Pt is the result of the coating as pre-treatment for EDX measurement. The morphology of C-SnO_2 NTs were further characterized by TEM and EDX measurement. Fig. 2a presents one SnO_2 nanotube among the C-SnO_2 NTs, and confirms the average diameter of *ca.* 200 nm. Also, the crystalline phase of SnO_2 (JCPDS 41-1445) is confirmed by the SAED patterns as shown in the inset of Fig. 2a. From the higher magnification TEM image (Fig. 2b), the SnO_2 nanotube consists of numerous nanoparticles and the wall thickness of the SnO_2 nanotube is *ca.* 20 nm. Fig. 2c shows the crystal domain of nanoparticles corresponding to lattice fringe of (110) and (101) at the end of the nanotube. As shown in Fig. 2e, the line-scan EDX elemental profile across an individual SnO_2 nanotube (as indicated direction in Fig. 2d) confirms the hollow structure.

The crystallographic structure of C-SnO_2 NTs was characterized by XRD in Fig. 3a. The crystalline phase is assigned to SnO_2 (JCPDS 41-1445) and Sn (JCPDS 04-0673), which indicates the partial reduction of SnO_2 during heat treatment under Ar atmosphere.[28-30] Thermogravimetric analysis (TGA) was conducted in air to determine the carbon content in C-SnO_2 NTs. As shown in Fig. 3b, the initial weight loss until 200 °C is the removal of physically adsorbed water, and then, the weight loss between 200 °C and 700 °C is attributed mainly to the oxidation of the carbon layer.[31,32] The carbon content of C-SnO_2 NTs except for the physically adsorbed water is determined to be *ca.* 19.6% by weight.

Electrochemical performance of C-SnO_2 nanotube arrays

To understand the reactive process of C-SnO_2 NTs and SnO_2 NPs, cyclic voltammetry (CV) was conducted in the voltage range of 0.01–2 V at a scan rate of 0.1 mV s^{-1} (Fig. 4a). The CV behavior is in good agreement with the results in previous reported C-SnO_2 anodes, indicating a similar electrochemical pathway.[33-35] In general, the electrochemical process of SnO_2-based anodes

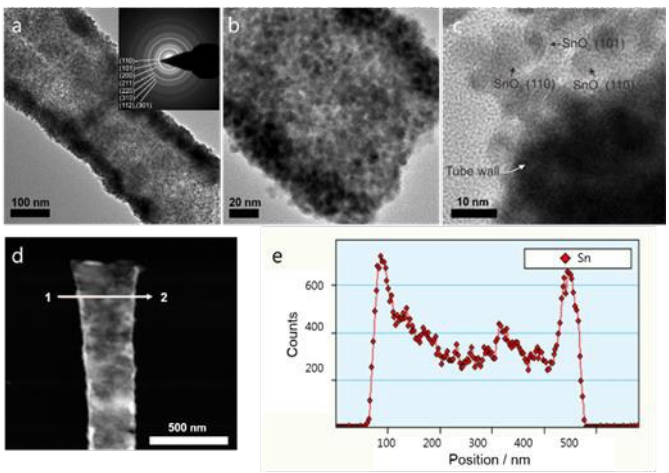

Fig. 2 (a)-(d) HR-TEM images of C-SnO_2 NTs and (e) line-scan EDX elemental profile across an individual SnO_2 nanotube as indicated direction in Fig. 2d.

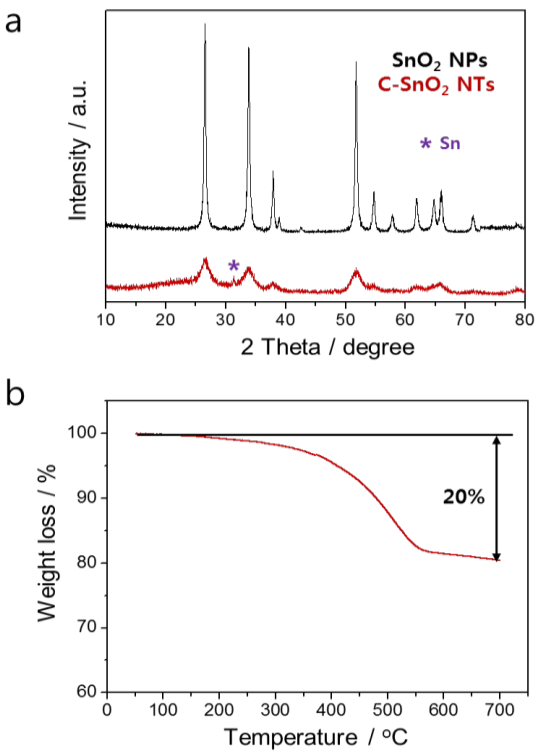

Fig. 3 (a) XRD pattern of C-SnO_2 NTs and SnO_2 NPs after heat treatment at 600 °C in Ar and (b) TGA analysis of C-SnO_2 NTs in air.

can be followed by two principal reactions:

$$SnO_2 + 4Li^+ + 4e^- \rightarrow Sn + 2Li_2O \quad (1)$$

$$Sn + xLi^+ + xe^- \rightarrow Li_xSn \ (0 \le x \le 4.4) \quad (2)$$

The first cathodic peak around 0.86 V is attributed to the reduction of SnO_2 to Sn and the formation of solid electrolyte interface (SEI) layer. In addition, the cathodic peaks at 0.01–0.7 V are due to the formation of Li_xSn alloys.[36,37] In the anodic peak at 0.56 V is attributed to the Li ion extraction from Li_xSn alloys, while that at 1.22 V is ascribed to the oxidation of Sn as the partial reversible reaction (1).[30,38] There was no significant difference between the C-SnO_2 NTs and SnO_2 NPs except for the peak position of reaction (1), showing a typical electrochemical behavior of SnO_2-based anodes.[3,33] A battery cell test was carried out to examine the potential of C-SnO_2 NTs as anode for LIBs. Fig. 4b presents the first two voltage profiles of C-SnO_2 NTs and SnO_2 NPs in the voltage range of 0.01–2 V at a current density of 0.1 A g^{-1}, which accords with the lithiation/delithiation process of SnO_2-based anode in previous reports.[33-35] The first discharge and charge capacities of the C-SnO_2 NTs are 1566 and 948 mAh g^{-1} and that of SnO_2 NPs are 2010 and 972 mAh g^{-1}, respectively. And, the second charge capacity of C-SnO_2 NTs and SnO_2 NPs is 897 and 922 mAh g^{-1}, respectively. From the charge capacity difference between the first and the second cycle compared with the first charge capacity, the capacity decreasing rate of C-SnO_2 NTs is close to that of SnO_2 NPs at first two cycle. The initial irreversible capacity of SnO_2-based anode materials comes from not only formation of SEI layer but also initial conversion reaction, which is not fully reversible. The C-SnO_2 NTs show a reasonably high coulombic efficiency (~61%) compared to other SnO_2-based anode materials.[28,35,39] Moreover, the voltage hysteresis in the charge and discharge curves of C-SnO_2 NTs is smaller than that of the SnO_2 NPs, suggesting that increased kinetic of electrodes of C-SnO_2 NTs which resulted from carbon coating.[34,39] Also, the suppressed plateau of C-SnO_2 NTs is observed, compared to that of SnO_2 NPs. The plateau in the potential range of 1.2 and 0.8 V comes from the formation of SEI layer and the conversion reaction between SnO_2 and Li ion, resulting in formation of Sn particle embedded in Li_2O matrix. Carbon coating can cause the decreasing resistance of lithiation/delithiation process, in addition, carbon itself can store the Li ions over wide range of potential.[34,40] Therefore, the C-SnO_2 NTs have higher (~1.4 V) and wide reaction potential. Furthermore, Some SnO_2 was reduced to Sn during heat treatment under Ar with carbon. These cause the suppression of plateau around 0.8 V in C-SnO_2 NTs. This similar features can be observed in other carbon and SnO_2 composite materials for LIBs.[28,34,35] The cycling performance of C-SnO_2 NTs and SnO_2 NPs at 0.1 A g^{-1} between 0.01 and 2 V is shown in Fig. 4c. Although the capacity decreasing rate of C-SnO_2 NTs is similar to that of SnO_2 NPs until the 10th cycle, C-SnO_2 NTs have a sta-

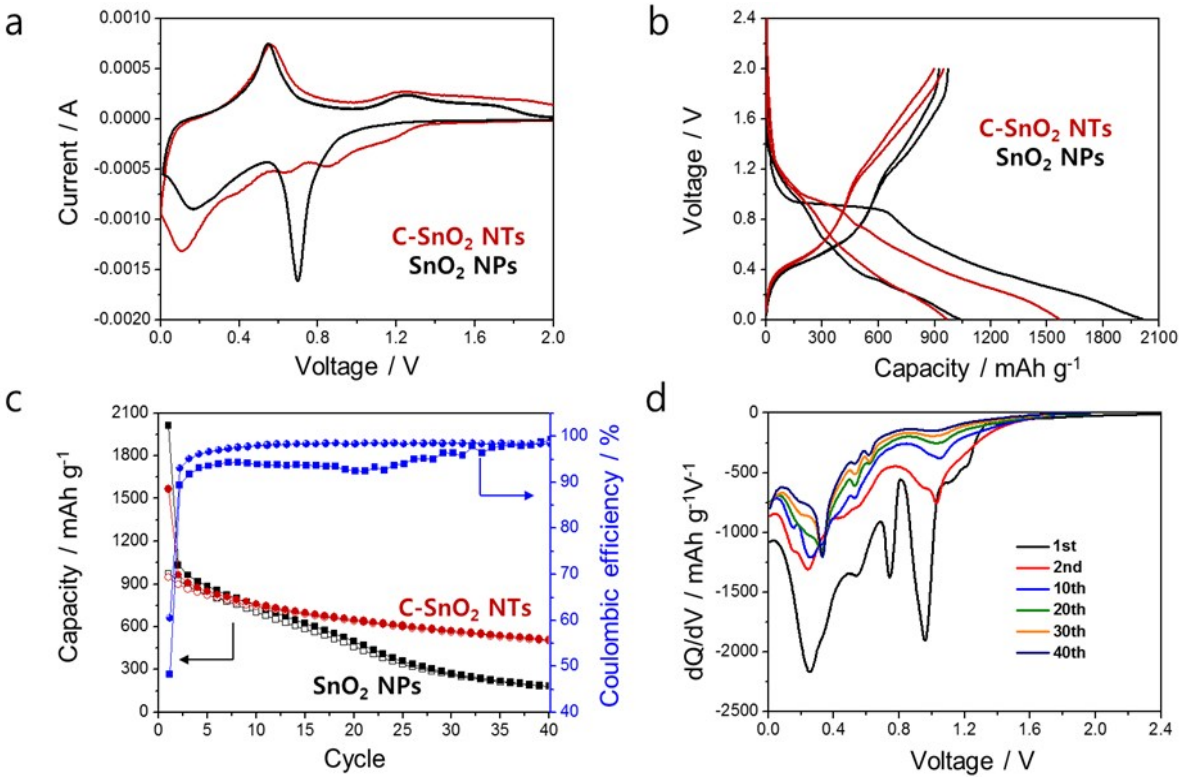

Fig. 4 (a) Cyclic voltammograms of C-SnO_2 NTs and SnO_2 NPs at the first cycle, (b) voltage profiles of C-SnO_2 NTs and SnO_2 NPs during the first two cycles at 0.1 A g^{-1}, (c) cycle performance of C-SnO_2 NTs and SnO_2 NPs at 0.1 A g^{-1} for 40 cycles with their coulombic efficiencies, and (d) dQ/dV profiles of C-SnO_2 NTs at 0.1 A g^{-1} at selected cycle.

ble capacity retention thereafter, and deliver a reversible capacity as high as *ca.* 500 mAh g^{-1} after 40 discharge/charge cycles. The high Li ion storage of C-SnO_2 NTs is better or comparable to that of SnO_2-based nanocomposites modified with carbon,[28,41,42] graphene,[39] or titanium nitride.[43] The coulombic efficiencies of C-SnO_2 NTs in Fig. 4c maintain a stable state, whereas that of the SnO_2 NPs exhibit an unstable condition fluctuating up and down over the whole cycles. The differential capacity profiles (dQ/dV *vs.* voltage) of C-SnO_2 NTs are shown in Fig. 4d. The distinct peaks between 0.01 and 0.7 V relate to the Li ion insertion reaction to form the Li_xSn alloys.[33,37] For the C-SnO_2 NTs, the intensities corresponding to the Li_xSn alloy peaks slowly diminish after the first cycle, and retain a stable area after 40 cycles, suggesting that a stable Li ion insertion is accomplished.

In Fig. 5a and b, the rate capability of C-SnO_2 NTs with different voltage cut-off condition was evaluated stepwise by increasing the current density. The better cycling stability is generally obtained by selecting the appropriate voltage cut-off condition, avoiding higher voltages (above 1 V) and also low voltages (near 0 V), when controlling the reversibility for the reaction of Li ions with SnO_2.[33,44] Especially in the higher (> 1.3) cut-off, Sn atoms aggregate from the destruction of Li_2O matrix, which leads to two phase reaction, volume mismatch, and eventually capacity fading.[44] In both cut-off condition, *ca.* 100 mAh g^{-1} of charge capacity decreases for the subsequent 5 cycles at the first 0.1 A g^{-1} step, and then the capacity becomes stable as the current density increases. When the current density is reduced back to 0.1 A g^{-1}, the C-SnO_2 NTs in both cut-off condition recover a respectable amount of the capacity at the first 0.1 A g^{-1} step, indicating an excellent rate capability. Moreover, the proportion of recovered capacity to the first 0.1 A g^{-1} step with 1.3 V cut-off is better than that with 1.5 V cut-off, which demonstrates again that the voltage limit influences the cycling stability. The coulombic efficiencies in both cut-off conditions are stable, and those with 1.3 V cut-off are slightly higher compared with 1.5 V cut-off except for the 1st and 26th cycles as shown in Fig. 5c. Fig. 5d indicates the last discharge/charge voltage profiles of each rate stage in Fig. 5b. As increased the current density, the lithiation potential decreases and the delithiation potential increases, which is attributed to the kinetic effects of electrode material.[45]

To elucidate the stabilizing effect of the C-SnO_2 NTs, the EIS measurement of C-SnO_2 NTs and SnO_2 NPs after the 5 and 40 cycles at a current density of 781 mAh g^{-1} was conducted (Fig. S2, ESI†). The plots consist of a depressed semicircle in the high to mid-frequency regions and a straight line in the low frequency region. The semicircle at high frequency can be assigned to the SEI film resistance (R_{SEI}), while that at mid-frequency is attributed to the charge transfer impedance on electrode/electrolyte interface (R_{ct}). And, the linear region corresponds to the semi-infinite diffusion of the Li ions in elect-

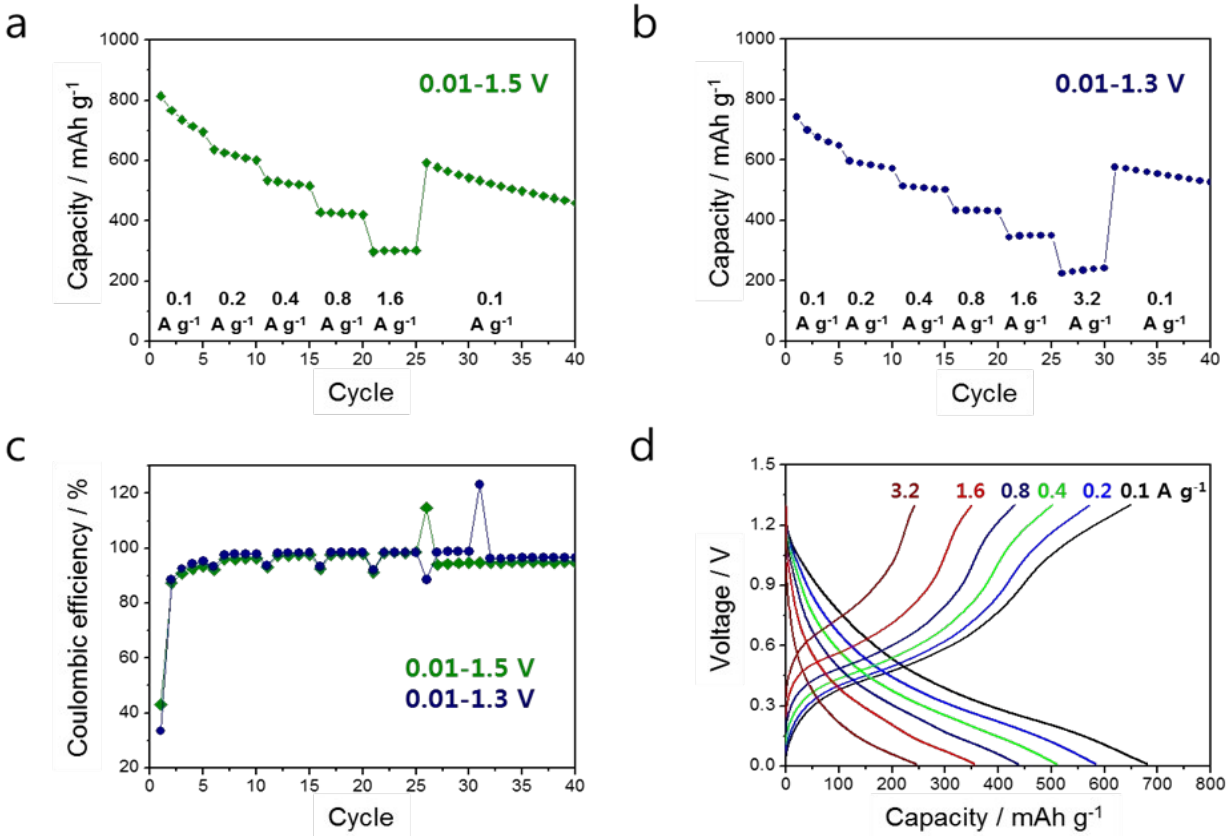

Fig. 5 Rate performance of C-SnO_2 NTs with cut-off voltage rage (a) 0.01-1.5 V and (b) 0.01-1.3 V, (c) coulombic efficiencies of 1.5 V and 1.3 V cut-off voltage, and (d) voltage profiles of C-SnO_2 NTs cycled at various current rates.

rode (R_e).[30,34] As observed, the semicircle diameter for C-SnO_2 NTs in the high to mid-frequency region are much smaller than that of SnO_2 NPs after the 40 cycles. Also, there is no obvious increase in the R_{SEI} of C-SnO_2 NTs between the 5 and 40th cycles, suggesting limited growth of the SEI layer in clear contrast to that of SnO_2 NPs. These results demonstrate that the C-SnO_2 NTs exhibit much lower contact and charge transfer resistance, implying its significantly enhanced charge transport in the nanotube.[30,34]

Conclusions

In summary, we fabricated SnO_2 nanotube arrays embedded in a carbon layer via a facile sol-gel synthesis using a polycarbonate membrane template, and investigated their electrochemical performance as an anode for LIBs. The carbon layer carbonized from polycarbonate at the top of the SnO_2 nanotubes plays a role in maintaining the 1D structure of individual SnO_2 nanotubes from the current collector to the top area facing separator. Such a binder- and carbon-free electrode, integrated with the current collector as a self-supporting anode, delivered a stable and high reversible capacity of 500 mAh g^{-1} at 0.1 A g^{-1} after 40 cycles, which is approximately 2.7 times higher than that of conventional powder electrode of SnO_2 nanoparticles. The high Li ion storage and stable capability are ascribed to the 1D hollow structure, alleviating the large volume changes of SnO_2 and reducing the diffusion path of electron and Li ion transport in the nanotube.

Acknowledgements

Y.-E. S. acknowledges the Institute for Basic Science (IBS) in Korea. This work was supported by Project Code (IBS-R006-G1). Y.-H. C. acknowledges financial support from the Priority Research Center Program (2009-0093814) and the Basic Science Research Program (2013R1A1A2061636) through the National Research Foundation of Korea (NRF), which is funded by the Ministry of Education.

Notes and references

[a] School of Chemical & Biological Engineering, Seoul National University, Seoul 151-742, Republic of Korea.

[b] Center for Nanoparticle Research, Institute for Basic Science (IBS), Seoul 151-742, Republic of Korea. E-mail: ysung@snu.ac.kr

[c] School of Advanced Materials Engineering, Kookmin University, Seoul 136-702, Republic of Korea. E-mail: yhun00@kookmin.ac.kr

1. M. Armand and J. M. Tarascon, *Nature*, 2008, **451**, 652.
2. C.-M. Park, J.-H. Kim, H. Kim and H.-J. Sohn, *Chem. Soc. Rev.*, 2010, **39**, 3115.
3. J. S. Chen and X. W. Lou, *Small*, 2013, **9**, 1877.
4. C. Zhu, X. Xia, J. Liu, Z. Fan, D. Chao, H. Zhang and H. J. Fan, *Nano Energy*, 2014, **4**, 105.
5. J. Qin, C. He, N. Zhao, Z. Wang, C. Shi, E.-Z. Liu and J. Li, *ACS Nano*, 2014, **8**, 1728.
6. C. Guan, X. Wang, Q. Zhang, Z. Fan, H. Zhang and H. J. Fan, *Nano Lett.*, 2014, **14**, 4852.
7. W. Ren, D. Kong, and C. Cheng, *ChemElectroChem*, 2014, DOI: 10.1002/celc.201402237.
8. R. Thomas and G. M. Rao, *J. Mater. Chem. A*, 2015, **3**, 274.
9. Z. Liu, J. Liu, J. Liu, L. Wang, G. Zhang and X. Sun, *Phys. Chem. Chem. Phys.*, 2014, **16**, 8808.
10. J. Chen, X.-H. Xia, J.-P. Tu, Q.-Q. Xiong, Y.-X. Yu, X.-L. Wang and C.-D. Gu, *J. Mater. Chem.*, 2012, **22**, 15056.
11. T. Mei, Y. Zhu, K. Tang and Y. Qian, *RSC Adv.*, 2012, **2**, 12886.
12. J. Guo, X. Chen and C. Wang, *J. Mater. Chem.*, 2010, **20**, 5035.
13. M. R. Zamfir, H. T. Nguyen, E. Moyen, Y. H. Lee and D. Pribat, *J. Mater. Chem. A*, 2013, **1**, 9566.
14. P. Meduri, C. Pendyala, V. Kumar, G. U. Sumanasekera and M. K. Sunkara, *Nano Lett.*, 2009, **9**, 612.
15. Y. Li, B. Tan and Y. Wu, *Nano Lett.*, 2008, **8**, 265.
16. N. Du, Y. Xu, H. Zhang, C. Zhai and D. Yang, *Nanoscale Res Lett*., 2010, **5**, 1295.
17. J. Wu, S. Lo, K. Song, B. K. Vijayan, W. Li, K. A. Gray and V. P. Dravid, *J. Mater. Res.*, 2011, **26**, 1646.
18. Y. Wang, J. Y. Lee and H. C. Zeng, *Chem. Mater*., 2005, **17**, 3899.
19. C. K. Chan, H. Peng, G. Liu, K. Mcilwrath, X. F. Zhang, R. A. Huggins and Y. Cui, *Nat. Nanotechnol*., 2008, **3**, 31.
20. T. D. Bogart, D. Oka, X. Lu, M. Gu, C. Wang and B. A. Korgel, *ACS Nano*, 2014, **8**, 915.
21. J.-Y. Gong, S.-R. Guo, H.-S. Qian, W.-H. Xu and S.-H. Yu, *J. Mater. Chem.*, 2009, **19**, 1037.
22. N. Du, H. Zhang, B. Chen, X. Ma, Z. Liu, J. Wu and D. Yang, *Adv. Mater*., 2007, **19**, 1641.
23. H. Tong, Y.-J. Zhu, L.-X. Yang, L. Li and L. Zhang, *Angew. Chem. Int. Ed.*, 2006, **45**, 7739.
24. H. Niu and M. Gao, *Angew. Chem. Int. Ed.*, 2006, **45**, 6462.
25. Z. Favors, W. Wang, H. H. Bay, A. George, M. Ozkan and C. S. Ozkan, *Sci. Rep*., 2014, **4**, 4605.
26. N. Li, C. R. Martin and B. Scrosati, *Electrochem. Solid-State Lett.*, 2000, **3**, 316.
27. J.-H. Wang, L.-H. Zhang, D.-H. Chen and Y.-Z. Guo, *Trans. Nonferrous Met. Soc. China*, 2007, **17**, s928.
28. P. Wu, N. Du, H. Zhang, J. Yu, Y. Qi and D. Yang, *Nanoscale*, 2011, **3**, 746.
29. F. D. Lupo, C. Gerbaldi, G. Meligrana, S. Bodoardo and N. Penazzi, *Int. J. Electrochem. Sci.*, 2011, **6**, 3580.
30. J. Fu, H. Qiao, D. Li, L. Luo, K. Chen and Q. Wei, *Sensors*, 2014, **14**, 3543.
31. I. Moreno, N. Navascues, M. Arruebo, S. Irusta and J. Santamaria, *Nanotechnology*, 2013, **24**, 275603.
32. N. Katiyar and K. Balasubramanian, *RSC Adv*., 2014, **4**, 47529.
33. I. A. Courtney and J. R. Dahn, *J. Electrochem. Soc.*, 1997, **144**, 2045.
34. N. R. Srinivasan, S. Mitra and R. Bandyopadhyaya, *Phys. Chem. Chem. Phys.*, 2014, **16**, 6630.
35. J. Li, Y. Zhao, N. Wang and L. Guan, *Chem. Commun.*, 2011, **47**, 5238.
36. K. Kravchyk, L. Protesescu, M. I. Bodnarchuk, F. Krumeich, M. Yarema, M. Walter, C. Guntlin and M. V. Kovalenko, *J. Am. Chem. Soc.*, 2013, **135**, 4199.
37. X. W. Lou, J. S. Chen, P. Chen and L. A. Archer, *Chem. Mater*., 2009, **21**, 2868.

38. Y. Yang, X. Ji, F. Lu, Q. Chena and C. E. Banks, *Phys. Chem. Chem. Phys.*, 2013, **15**, 15098.
39. X.-T. Chen, K.-X. Wang, Y.-B. Zhai, H.-J. Zhang, X.-Y. Wu, X. Wei and J.-S. Chen, *Dalton Trans.*, 2014, **43**, 3137.
40. M. Noh, Y. Kwon, H. Lee, J. Cho, Y. Kim and M. G. Kim, *Chem. Mater*., 2005, **17**, 1926.
41. K. E. Aifantis, S. Brutti, S. A. Hackney, T. Sarakonsria and B. Scrosati, *Electrochimica Acta*, 2010, **55**, 5071.
42. X. W. Guo, X. P. Fang, Y. Sun, L. Y. Shen, Z. X. Wang and L. Q. Chen, *J. Power Sources*, 2013, **75**, 226.
43. M. Liu, X. Li, H. Ming, J. Adkins, X. Zhao, L. Su, Q. Zhoub and J. Zheng, *New J. Chem.*, 2013, **37**, 2096.
44. I. A. Courtney and J. R. Dahn, *J. Electrochem. Soc.*, 1997, **144**, 2943.
45. H.-W. Lee, P. Muralidharan, R. Ruffo, C. M. Mari, Y. Cui and D. K. Kim, *Nano Lett.*, 2010, **10**, 3852.